

Human milk-derived peptide MDABP ameliorates hyperoxia lung damage via inhibiting the ferroptosis signaling pathway

Linjie Liu¹, Yun Qian¹, Ziwei Yu¹, Huimin Li, Jingjing Chen, Heng Dou, **Shushu Li**^{*}, Jing Yin^{*}, Shuping Han^{*}

Department of Pediatrics, Women's Hospital of Nanjing Medical University, Nanjing Women and Children's Healthcare Hospital, Nanjing, China

ARTICLE INFO

Keywords:

Bronchopulmonary dysplasia
MDABP
Hyperoxia
Ferroptosis

ABSTRACT

Human breast milk, the best source of nutrition for newborns, can reduce the incidence of bronchopulmonary dysplasia (BPD). Bioactive peptides are important components of human breast milk. However, their function in BPD are unclear. We screened a novel peptide (named MDABP) in the breast milk of mothers of premature infants, which has beneficial effects in experimental BPD. This study aimed to investigate the role and mechanism of MDABP *in vivo* and *in vitro*. Newborn Sprague-Dawley (SD) rats were exposed to normoxia (21 % O₂) or hyperoxia (85 % O₂) and injected with MDABP or PBS from postnatal days 1 to 7 (PN1-PN7). On PN7, the lungs were harvested for histological and biochemical analysis. The results revealed that MDABP improved alveolar simplification and pulmonary vascular retardation, promoted alveolar epithelial cell (AEC) proliferation and inhibited cell apoptosis. *In vitro*, MDABP, but not scrambled MDABP, promoted cell proliferation and reduced cell injury without obvious toxicities. RNA-sequencing in A549 cells showed a total of 214 genes were significantly differentially expressed between the MDABP + hyperoxia and hyperoxia groups, including 80 upregulated and 134 downregulated genes. KEGG pathway analysis showed that significant differentially expressed genes were related to the ferroptosis signaling pathway. Rescue experiments showed that MDABP reduced the hyperoxia- and ferroptosis-induced damage to AEC by decreasing the levels of Fe²⁺ and ROS and increasing the levels of GSH and GPX4. The p-value of the above experiment was less than 0.05, which was considered statistically significant. This study provides a new basis for developing treatments for BPD.

1. Introduction

Bronchopulmonary dysplasia (BPD) is a chronic lung disease with multifactorial etiology. In premature infants, the lungs are still in the developmental stage and are thus vulnerable to environmental factors. Long-term oxygen therapy, especially when administered at high oxygenation levels, is a significant risk factor for the development of BPD (Deng et al., 2023). BPD is characterized by impaired alveolarization and abnormal pulmonary vascular development (Gilfillan et al., 2021). The survival rates of neonates, particularly those born extremely premature, have continuously improved in recent years due to advancements in perinatal treatment technology (Thébaud et al., 2019). Meanwhile, the incidence of BPD has also increased over time. Research suggests that the incidence of BPD is up to (Bell et al., 2022)9.8 %. Current treatments for BPD are mainly supportive, and there have been no breakthroughs in progress. Therefore, it is an urgent problem to find

reliable ways to alleviate or intervene in BPD.

In recent years, some bioactive peptides, such as apelin (Visser et al., 2010); erythropoietin-derived peptide (Liu et al., 2017) and calcitonin gene-related peptide (CGRP) (Dang et al., 2017), have been identified to have important functions in attenuating hyperoxia-induced lung injury. Human breast milk is known as the best source of nutrition to support infant growth and development, not only because of its composition of proteins, carbohydrates and lipids, but also its various other biologically active components (Yi and Kim, 2021). A large number of studies has revealed that breastfeeding decreases the incidence of BPD and that active ingredients in breast milk play a major role in this association (Huang et al., 2019; Villamor-Martínez et al., 2018). Bioactive peptides are an important part of the anti-infective properties of breast milk (Fu et al., 2017), as well as its benefits to immune regulation, and promotion of growth and development (Hamley, 2017). The peptides are characterized by their small molecular weights and easy absorption. All of

* Corresponding authors.

E-mail addresses: lishushu@njmu.edu.cn (S. Li), yinjing826@126.com (J. Yin), shupinghan@njmu.edu.cn (S. Han).

¹ These authors contributed equally to this work.

<https://doi.org/10.1016/j.jff.2024.106036>

Received 28 August 2023; Received in revised form 10 January 2024; Accepted 21 January 2024

Available online 1 February 2024

1756-4646/© 2024 The Author(s). Published by Elsevier Ltd. This is an open access article under the CC BY-NC-ND license (<http://creativecommons.org/licenses/by-nc-nd/4.0/>).

these studies indicate that the further research into the bioactive peptides found in breast milk is expected to provide new ideas for the treatment of BPD.

Based on theoretical support and polypeptide analysis of the colostrum of mothers with premature infants, in our previous paper, we identified a novel immunoglobulin-derived polypeptide that retained the functional region of its source protein (Wang et al., 2019). Then, we conducted functional verification *in vitro* and *vivo*, and found that it promoted the proliferation of alveolar epithelial cells (AEC), inhibited cell apoptosis, and increased the expression of the type I and type II AEC markers AQP5 and SP-C. We further revealed that MDABP alleviated AEC damage by inhibiting the ferroptosis signaling pathway. Our findings provide the basis to propose a novel candidate drug that alleviates AEC injury and may be a potential therapeutic approach for the treatment of BPD.

2. Materials and methods

2.1. Acquisition of peptides

The synthetic peptide MDABP comprising amino acids (aa) 20–38 of human breast milk immunoglobulin (QSVLTQPPSVSAAPGQKV), a scrambled version of MDABP (SPQQPGVVASTKQPSLVA) and fluorescein isothiocyanate (FITC)-labeled MDABP (FITC-MDABP) were obtained from Science Peptide Biological Technology Co, Ltd (Shanghai, China). Bioactive peptides were endotoxin free and synthesized via solid-phase technology. The purity of the peptides was determined by reverse-phase high-performance liquid chromatography (HPLC) and exceeded 95 %. Stock solutions of peptides were distilled with deionized water (Thermo, USA) and stored at -80°C . The properties of MDABP were calculated with the ProtParam tool from the ExPASy server (Cai et al., 2021).

2.2. Cell culture and the localization of MDABP in cells

A549 cells (human alveolar epithelial cells) were obtained from the Chinese Academy of Sciences. The cells were cultured in Dulbecco's modified eagle medium (DMEM)/F12 medium (Gibco, USA) containing 10 % fetal bovine serum (FBS) (Gibco, USA) and 1 % penicillin streptomycin (Gibco, USA) at 37°C containing 5 % CO_2 . A549 cells were cultured in a special hyperoxic cell culture chamber with 85 % O_2 and 5 % CO_2 at 37°C to simulate the BPD state, while control cells were cultured in 21 % O_2 and 5 % CO_2 . After treated with FITC-MDABP (1 μM) for 2 h, A549 cells were fixed with 4 % polyformaldehyde and stained with DAPI. Then, photographs were taken using a fluorescence microscope (Zeiss, Germany).

2.3. Cell viability assay

The cell counting kit-8 (CCK-8) assay was used to detect cell viability. A549 cells (3×10^3 cells/well) were seeded into a 96-well culture plate for 24 h and then incubated with different concentrations of MDABP for 24 h. Afterward, the cells were cultured with a mixture (1:10) of CCK-8 detection reagent (APExBio, USA) and serum-free DMEM/F12 medium for 2 h at 37°C containing 5 % CO_2 . The absorbance at 450 nm was measured by a microplate reader.

2.4. Cell proliferation

A549 cells were plated on a 6-well plate at a concentration of 1.5×10^5 cells/well and incubated overnight. The A549 cells were then treated with hyperoxia (85 % O_2) and MDABP (1 $\mu\text{mol/L}$) for 36 h. Then, a BeyoClick™ EdU-488 kit (Beyotime, China) was used to detect cell proliferation following the manufacturer's instructions. Firstly, the cells were incubated with EdU for 2 h at 37°C . Then they were washed by PBS for three times and fixed with 4 % paraformaldehyde. After incubating

with 0.3 % Triton X-100, the cells were successively stained with Click Additive Solution and DAPI. Finally, photographs were taken using a fluorescence microscope (Zeiss, Germany).

2.5. Measurement of intracellular free iron levels

The intracellular free iron levels were measured with FerroOrange (Dojindo, Japan), a fluorescent probe specific for the detection of labile iron Fe (II). The A549 cells were seeded at a concentration of 2×10^3 cells/well in a black 96-well microplate and incubated overnight. Then, the A549 cells were treated with hyperoxia, MDABP (1 $\mu\text{mol/L}$) or RSL3 for 36 h, and incubated with 1 μM FerroOrange for 0.5 h. The fluorescence intensity was measured with a fluorescence microscope (Zeiss, Germany) with FerroOrange.

2.6. Measurement of GSH levels

Intracellular GSH concentration was measured using a GSH assay kit (Wanleibio, Shenyang, China). The assay was carried out according to the kit instructions after 36 h of treatment. In brief, we added reagent 1 to the cell supernatant and centrifuged for 10 min at 3500 rpm. Then the supernatant mixed with reagent 2 and 3, respectively. The absorbance was determined by fluorescence microplate, and the GSH content was calculated according to OD value.

2.7. Measurement of ROS generation

A549 cells were seeded at a concentration of 1.5×10^5 cells/well in a 6-well plate and incubated overnight. A549 cells were treated with MDABP, RSL3, or hyperoxia for 36 h. The fluorescent dye 2',7'-dichlorodihydrofluorescein diacetate (DCFH-DA; Beyotime, China) was used as a probe to detect intracellular ROS levels. According to the manufacturer's instructions, the probe (10 μM) was loaded in A549 cells about 30 min. The fluorescence intensity was measured with a microplate reader at an excitation wavelength of 488 nm and an emission wavelength of 525 nm. The ROS expression level was calculated as the ratio of the fluorescence intensity to the number of cells in each group.

2.8. Animal models and treatment

In the term Sprague-Dawley (SD) rat model of BPD, lung development in pups from embryonic day 18 to postnatal day 5 (E18 to PN5) in pups resembled that from 24 to 38 weeks of gestational age in preterm infants (Giusto et al., 2021). Thus, we selected newborn SD rats as the BPD animal model. All pregnant SD rats were obtained from the Experimental Animal Center of Nanjing Medical University (Nanjing, China). All animal experiments were approved by the Animal Research and Care Committee of Nanjing Medical University (Approval number: IACUC-1907021). Neonatal SD rats were randomly divided into three groups: newborn SD rats and their mothers in normoxia (21 % O_2) served as the control group (CTL); the hyperoxia group (HYP) and their mothers, the hyperoxia + peptide group (HYP + MDABP) and their mothers, were kept in a cage in a sealed plexiglass chest. The HYP + MDABP group received intraperitoneal injections of MDABP at a concentration of 10 mg/kg. The BPD model was induced in the newborn rats by exposing them to high oxygen (85 % O_2) as previously described (Zhou et al., 2022). The adult animals were allowed two hours of recovery in room air every day to prevent excessive oxygen toxicity. Male and female pups were randomly assigned to maintain a 1:1 ratio. The litter size was controlled at 12 ± 2 pups; and the average weight difference was ± 1 g. The body weights of the rat pups were measured every day. All pups were euthanized at day 7, and lung tissues were harvested for further analysis.

Table 1
Primer sequences for real-time quantitative PCR.

Target	Primer sequence (5'–3') (F: Forward; R: Reverse)
human-GAPDH	F: GGAGCGAGATCCCTCCAAAAT R: GGCTGTTGTCTACTTCTCATGG
human-AQP5	F: GCCACCTTGTTCGGAATCTACT R: GGCTCATACGTGCCTTTTGATG
human-SP-C	F: GAGATGAGCATCGGAGGAGC R: AGGAGCCGCTGGTAGTCATA
Rat-GAPDH	F: AGGTCGGTGTGAACGGATTTG R: TGTAGACCATGTAGTTGAGGTCA
Rat-AQP5	F: CCCAAGGCCACCATGAAGAA R: TATGGCCAGGCCAAAGGCTA
Rat-SP-C	F: ATGGAGAGTCCACCGGATTAC R: ACCACGATGAGAAGGCGTTTG
Rat-IL-6	F: AGCGATGATGCATGTGCAGA R: GGAACTCCAGAAGACCAGAGC
Rat-IL-1 β	F: CCAGGATGAGGACCCAAGCA R: TCCCGACCATTGCTGTTTCC
Rat-TNF- α	F: CTCAAAACCTCGAGTGACAAGC R: CCGTGATGCTAAGTACTTGG

Glyceraldehyde-3-phosphate dehydrogenase (GAPDH); Aquaporin 5 (AQP5); Surfactant protein C (SP-C); Interleukin-6 (IL-6); Interleukin-1 β (IL-1 β); Tumor Necrosis Factor alpha (TNF- α).

2.9. Histopathological analysis

The lungs of each rat were subjected to immersion in 4 % paraformaldehyde, fixing in paraffin, and sectioning at 5 μ m. Sections were stained with hematoxylin and eosin (H&E) and evaluated by light microscopy.

2.10. . Immunofluorescence staining and vWF immunohistochemistry

To assess AEC proliferation in the lung after hyperoxia, lung tissues were stained for Ki67 (proliferative marker) and SP-C (marker of type II alveolar epithelial cells). Briefly, lung sections were deparaffinized and rehydrated. For antigen retrieval, lung sections were exposed to 10 mM citrate buffer (pH 6, Servicebio, G1202, China) at 90–120 °C for 25 min.

Subsequently, tissue sections were treated with blocking solution at room temperature for 1 h. Lung sections were incubated with the primary antibodies rabbit anti-Ki67 (Servicebio, GB111141, China, 1:400) and rabbit anti-SP-C (Servicebio, GB25303, China, 1:400) in the dark at 4 °C overnight. Following washing steps with $1 \times$ PBS, sections were stained with Alexa Fluor 488-conjugated secondary antibody (Servicebio, GB27303, China, 1:400) and Cy3-conjugated secondary antibody (Servicebio, GB21303, China, 1:300) at room temperature for 2 h. After a final washing step, sections were mounted with DAPI (Vector Labs, California, 1:1000) and quantified for cells positive for Ki67 and SP-C.

Similarly, 5 μ m paraffin-embedded lung sections were stained overnight with a primary antibody against vWF (Sigma, AB7356, 1:250) at 4 °C. Following three washing steps with 1 \times PBS, sections were analyzed for vWF-positive vessel density.

2.11. RT-qPCR analysis

Total RNA was obtained from cultured A549 cells or fresh lung tissue using TRIzol Reagent (Takara, Japan) and reverse transcribed into cDNA with a reverse transcription kit (Vazyme, Nanjing, China) according to the manufacturer's instructions. AQP5, SP-C, IL-6, IL-1 β , TNF- α and GAPDH mRNA expression levels were quantified with a ViiA7 Real-Time PCR system (Life Technologies, USA). The sequences of the primers are listed in [Table 1](#). GAPDH was used as the internal control, and the relative expression levels of the target genes were calculated according to the $2^{-\Delta\Delta C_t}$ method.

2.12. Protein extraction and Western blotting

A549 cells and lung tissues subjected to different treatments were lysed in RIPA buffer containing protease inhibitor cocktail and phosphatase inhibitor cocktail (APExBIO, USA). The lung tissues were further homogenized with a homogenizer. Then, the lysates were centrifuged at 12000 rpm and 4 °C for 30 min. The protein concentration was measured with a BCA kit (Thermo Fisher Scientific, USA). Equal amounts of proteins were separated by gel electrophoresis, and transferred to PVDF membranes (Millipore, Billerica, MA, USA). The

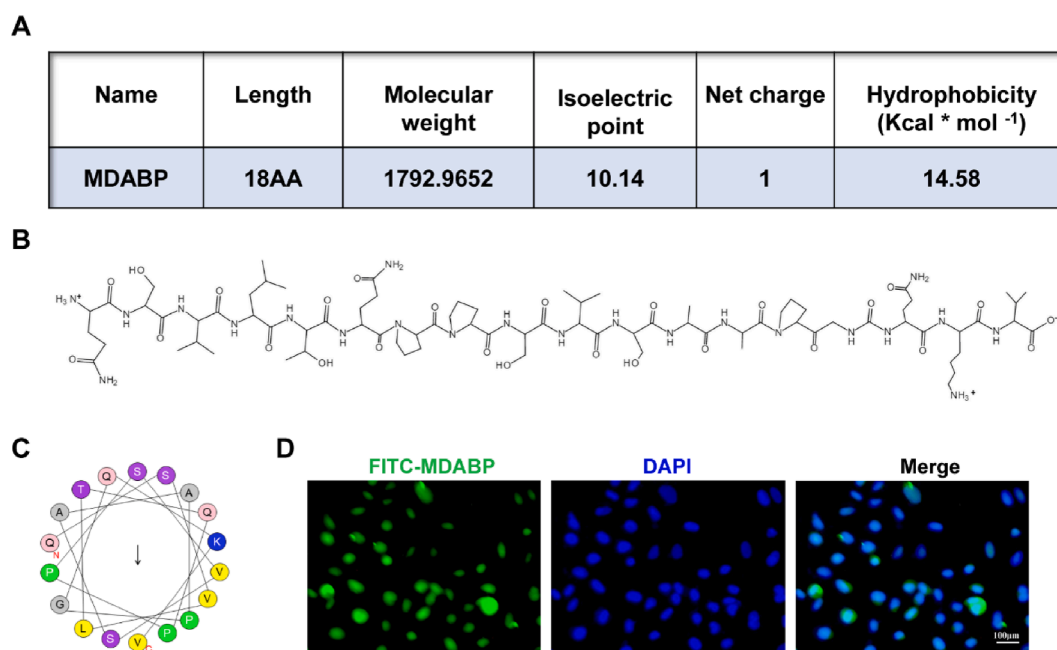


Fig. 1. Biological characterization of peptide MDABP. (A-B) Basic physical and chemical properties and amino sequence of peptide MDABP; (C) Helical wheel projections of MDABP (<http://heliquest.ipmc.cnrs.fr/>). (D) Fluorescence microscope images of A549 cells treated with FITC-MDABP. A549 cells were incubated with FITC-MDABP (green) at 37 °C for 2 h before imaging. Nuclei were stained with DAPI (blue) before imaging. The magnification of these images was 400 ×. (For interpretation of the references to colour in this figure legend, the reader is referred to the web version of this article.)

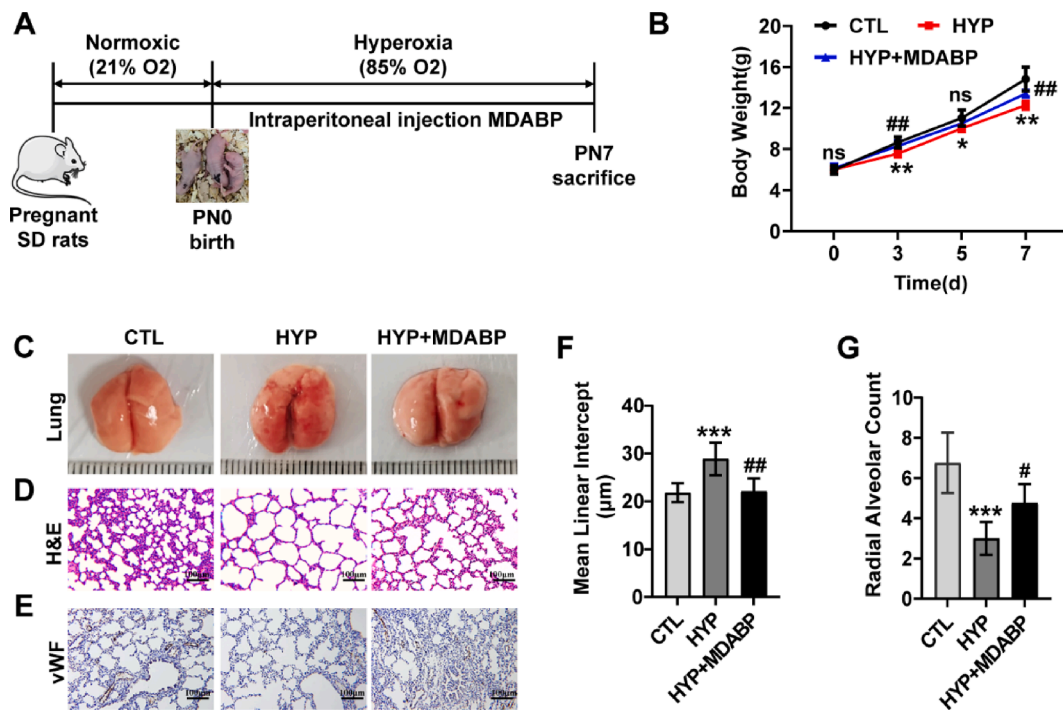


Fig. 2. MDABP improved the pathological changes in animal models of BPD. The pregnant SD rats were kept in room air until delivery. Then, the newborn mice were immediately exposed to 85 % hyperoxia for 7 days to establish the BPD model. Meanwhile, 10 mg/kg MDABP was intraperitoneally injected into BPD model mice. (A) Flow chart showing the BPD model. (B) Body weights were recorded at 0, 3, 5 and 7 days after birth. (C-E) The morphology of lung tissue, H&E staining and vWF immunostaining are shown in the control, hyperoxia and hyperoxia treated with MDABP groups. The endothelial cell marker vWF showed the development of pulmonary microvessels in newborn mice. Summary data of the quantitative histomorphometric analysis: mean linear intercept (MLI) (F) and radial alveolar count (RAC) (G). Scale bars, 100 μ m. Data are reported as the means \pm SDs, $n \geq 6$, */ $\#$ $P < 0.05$, **/ $\#\#$ $P < 0.01$, ***/ $\#\#\#$ $P < 0.001$, ns ≥ 0.05 , * vs control group (CTL), # vs hyperoxia group (HYP).

membranes were blocked 5 % skim milk at room temperature for 2 h and then incubated with the following primary antibodies at 4 °C overnight: anti-SP-C (Affinity, 1:1000 dilution), anti-AQP5 (Wanleibio, 1:500 dilution), anti-VEGF-A (Proteintech, 1:1000 dilution), GPX4 (Proteintech, 1:1000 dilution), anti-GAPDH (Proteintech, 1:5000 dilution). The membranes were washed with Tris-buffered saline Tween-20 (TBST) three times, and then incubated with HRP-conjugated secondary antibodies (goat antirabbit or goat antimouse IgG; Proteintech 1:5000) at room temperature for 1 h. GAPDH expression was used as an internal control. The blots were developed with an enhanced chemiluminescence detection kit and the images were captured with Imager-Tanon. Finally, ImageJ software was used to quantify the data.

2.13. RNA sequencing

To further explore the underlying mechanisms of the protective functions of MDABP, RNA sequencing was performed to compare the mRNA expression profile between the HYP and HYP + MDABP groups. Total RNA was extracted from A549 cells using an RNeasy kit (Vazyme, Nanjing, China). The RNA quality and quantity were assessed using an Agilent 2100 bioanalyzer (Agilent Technologies, USA). After RNA quality control, double-stranded cDNA was synthesized from RNA by reverse transcription and then end-repaired. The cDNA was amplified and purified by RT-qPCR, followed by quality testing for library screening. The qualified cDNA libraries were sequenced using Illumina HiSeq™ platform according to the manufacturer's instructions. The raw sequencing were subjected to bioinformatics analysis. The mRNAs with | fold change | ≥ 1.5 and p value < 0.05 were considered as significantly differentially expressed. The DEGs were further annotated and enriched for Gene Ontology (GO) and Kyoto Encyclopedia of Genes and Genomes (KEGG) pathway using Cluster Profiler R v3.8.1 and KOBAS v3.0.3.

2.14. Statistical analysis

The experimental data were analyzed by ImageJ and GraphPad Prism 8.0 Software. Data were represented as the mean \pm standard deviation (SD). In each group, more than three parallel samples were collected and the mean and SD were calculated. In each experiment, there was independently repeated at least three times, and Statistics were analyzed by the average value and standard error of parallel samples. An unpaired two-tailed Student's t -test were used for pairwise comparison between each group of data. $P < 0.05$ was considered statistically significant.

3. Results

3.1. Biological characterization of the peptide MDABP

MDABP is an 18-amino acid peptide with a molecular weight of 1.79 kDa. The basic information and primary structure of the peptide MDABP are shown in Fig. 1A-B. The amphipathicity of MDABP was determined using helical wheel projections to show the distribution of hydrophobic and hydrophilic amino acids (Fig. 1C). To investigate the membrane permeability and subcellular distribution of MDABP, A549 alveolar epithelial cells were incubated with FITC-tagged MDABP for 2 h and analyzed using a fluorescence microscope. As shown in Fig. 1D, tagged MDABP penetrated the cell membrane and was observed in both the cytoplasm and nucleus, displaying no sign of specific intracellular localization.

3.2. MDABP improved lung tissue injury in a mouse model of BPD

Long-term exposure to high oxygen levels is one of the most important factors causes of BPD (Dakshinamurti, 2022). Thus, we

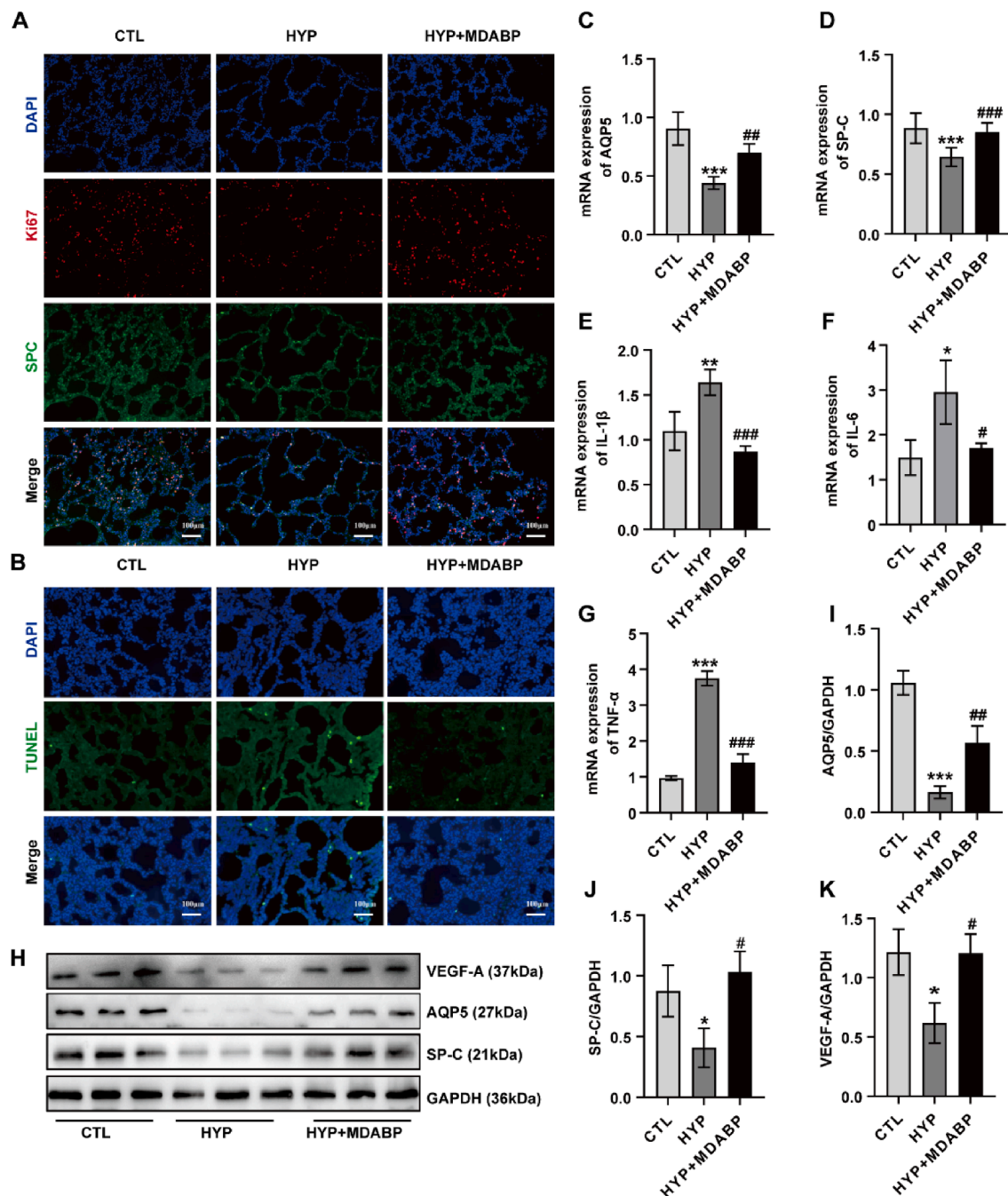


Fig. 3. The function of MDABP in animal models of BPD. Ki67 and TUNEL staining were performed on whole lung sections from (PN7 mice). (A) Ki67 and SP-C double immunofluorescence staining showed that MDABP promoted alveolar epithelial cell proliferation. (B) TUNEL staining showed that MDABP ameliorated hyperoxia (HYP)-induced apoptosis. The mRNA expression levels of AQP5 and SP-C and the protein expression levels of AQP5, SP-C and VEGF-A in animal models of BPD were measured by RT-qPCR (C-D) and Western blotting (H-K) after treatment with 10 mg/kg MDABP. The levels of IL-1 β , IL-6, and TNF- α were measured by RT-qPCR in lung tissues from mouse BPD models of MDABP treatment (E-G). Scale bars, 100 μ m. Data are reported as the means \pm SDs, $n \geq 6$, */# $P < 0.05$, **/## $P < 0.01$, ***/### $P < 0.001$, ns ≥ 0.05 , * vs control group (CTL), # vs hyperoxia group (HYP).

established a murine model of BPD through postnatal hyperoxia, which is depicted in Fig. 2A. The body weight of the hyperoxia-treated mice was reduced by an average of 17.3 % at PN7 compared to control mice reared under normoxic conditions. Meanwhile, the body weight of the MDABP-treated pups was increased by an average of 9.2 % compared to the hyperoxia group (Fig. 2B). Compared to the hyperoxia group, the MDABP-treated rat pups showed attenuated lung tissue collapse and inflammatory infiltration (Fig. 2C). Histological analysis revealed that alveolar and microvessel development were impaired in the hyperoxia group, as evidenced by a significantly decreased number of pulmonary

alveoli, reduced expression of the endothelial cell marker vWF and enlarged, simplified alveoli. However, these effects were improved in MDABP-treated rat pups (Fig. 2D–G).

3.3. The function of MDABP in a mouse model of BPD

To further study the effects of the peptide MDABP, immunofluorescence staining of rat pup lungs was performed. The results showed that MDABP treatment improved the inhibition of Ki67 and the increase in apoptosis (shown by TUNEL staining) induced by high oxygen exposure

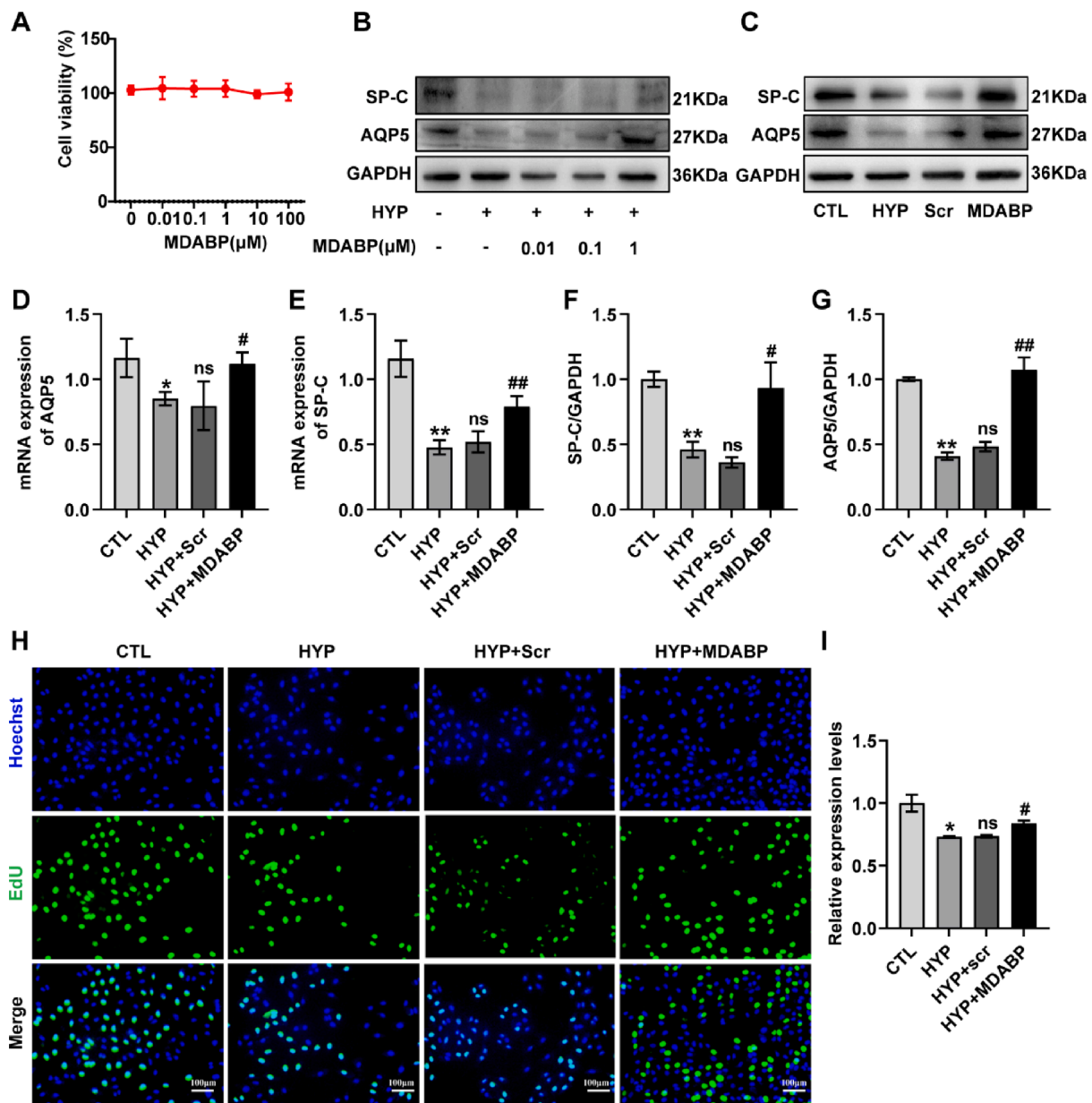


Fig. 4. MDABP can reduce A549 cell damage induced by hyperoxia and promote proliferation. (A) The cell viability of A549 cells treated with different concentrations of MDABP was examined by CCK-8 assay. (B) The expression of AQP5 and SP-C in A549 cells was measured by Western blotting after treatment with different concentrations of MDABP for 36 h. (C–G) The expression levels of AQP5 and SP-C in A549 cells was measured by Western blot and RT- qPCR after treatment with 1 μM MDABP for 36 h. (H–I) Cell proliferation was measured by a BeyoClick™ EdU-488 kit, and the image magnification was 200 ×. Data are presented as the mean ± SD, $n \geq 3$, */# $P < 0.05$, **/## $P < 0.01$, ns ≥ 0.05 , * vs control group (CTL), # vs hyperoxia group (HYP).

(Fig. 3A and B). Compared with BPD mice, the qPCR results showed that the mRNA expression levels of AQP5 (the marker of AT I) and SP-C (the marker of AT II) were increased (Fig. 3C and D) and MDABP treatment also ameliorated the protein expression levels of AQP5, SP-C and VEGF-A (the marker of pulmonary vascular endothelial cells) in BPD mice (Fig. 3H–K). In addition, the levels of IL-1β, IL-6, and TNF-α were significantly lower in lung tissues from mice with BPD treated with MDABP (Fig. 3E–G).

3.4. MDABP ameliorated damage to alveolar epithelial cells in vitro

Human A549 alveolar epithelial cells were selected to evaluate the effect of MDABP *in vitro*. A549 cells were incubated with different concentrations of MDABP for 36 h, and MDABP showed no cytotoxicity (Fig. 4A). Subsequently, we measured the protein expression of SP-C and

AQP5, which were significantly higher in the 1 μM MDABP treatment group than in the BPD group (Fig. 4B). To further determine whether MDABP is beneficial to alveolar epithelial cells, we treated hyperoxia-exposed A549 cells with 1 μM MDABP or 1 μM scrambled-MDABP for 36 h, and assessed the protein expression levels, mRNA expression levels, and cell proliferation. The results indicated that MDABP significantly promoted the mRNA and protein expression levels of alveolar epithelial cells (Fig. 4C–G) and reduced the inhibition of A549 cell proliferation caused by hyperoxia exposure (Fig. 4H and I). However, scrambled peptide treatment had none of the above effects.

3.5. Differential gene expressions (DEGs)

The gene expression profiles of hyperoxia and MDABP-treated A549 cells were analyzed by RNA sequencing (RNA-seq) to explore the

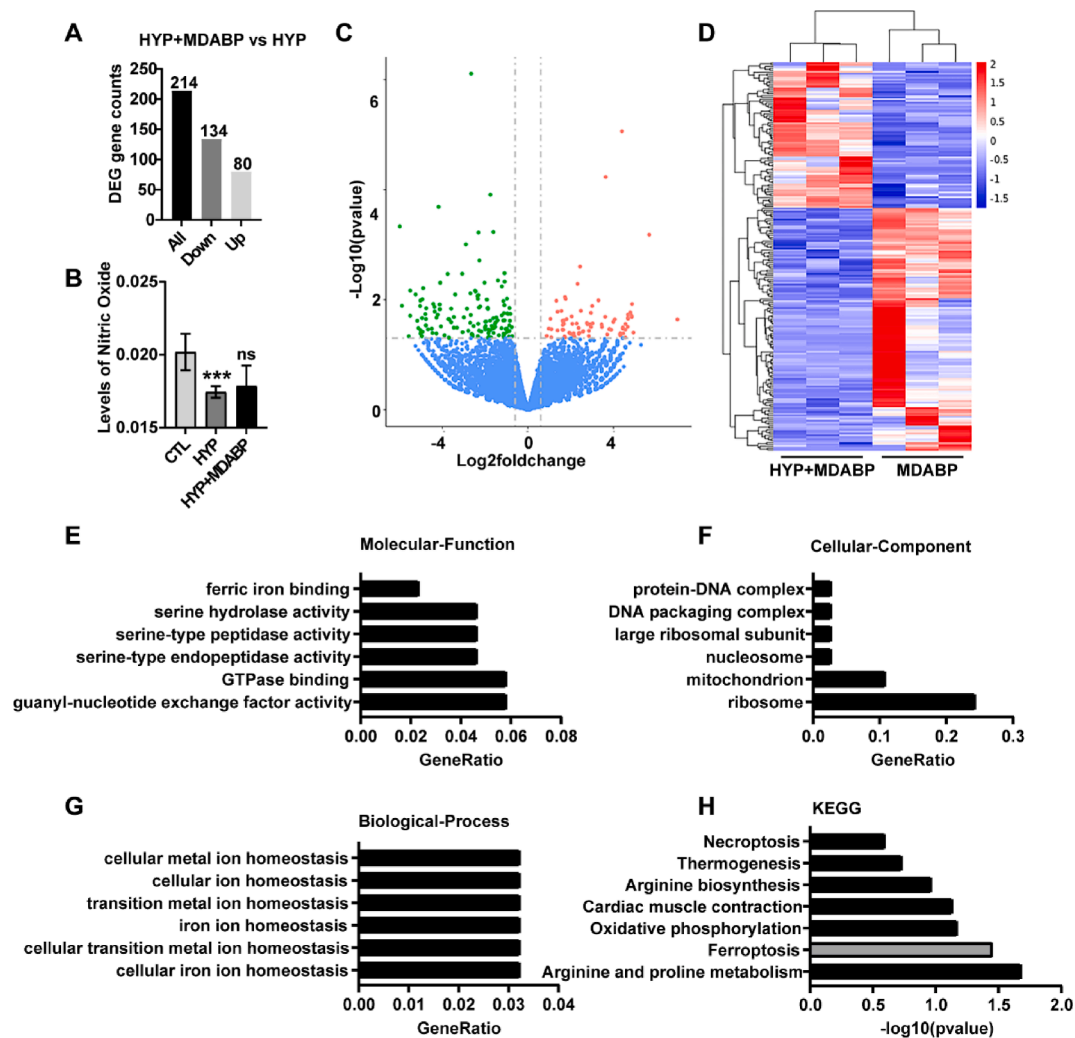


Fig. 5. Identification of differentially expressed mRNAs after MDABP treatment in A549 cells. (A) The number of differentially expressed genes. (B) Analysis of nitric oxide levels in the arginine and proline metabolism pathways. (C) Volcano plot showing the significantly differentially expressed genes identified in the two groups. (Red dots indicate significantly upregulated genes; green dots indicate significantly downregulated genes). (D) Heatmap analysis of the genes. (E–G) GO analysis and (H) KEGG pathway analysis. *** $P < 0.001$, ns ≥ 0.05 ; CTL: control group; HYP: hyperoxia group; HYP + MDABP: hyperoxia group treated with peptide MDABP. (For interpretation of the references to colour in this figure legend, the reader is referred to the web version of this article.)

molecular mechanism underlying MDABP treatment. We identified 214 genes with significant differential expression ($|\text{Fold-change (FC)}| \geq 1.5$ and $q\text{-value} \leq 0.05$) and visualized them in a volcano plot (Fig. 5A, C). We performed a hierarchical clustering analysis of differentially expressed mRNAs between the hyperoxia (HYP) and MDABP-treated (HYP + MDABP) groups using a heatmap (Fig. 5D). The two groups showed similar expression patterns and clustered together. Gene Ontology (GO) enrichment analysis was used to annotate the potential functions of DEGs. Molecular function analysis showed that the DEGs were involved in the guanylate and serine metabolism processes, as well as ferric iron binding (Fig. 5E). Cellular component analysis showed that DEGs were significantly enriched in ribosomes and mitochondria components (Fig. 5F). Biological process analysis revealed an enriched GO term related to cellular iron homeostasis (Fig. 5G). KEGG pathway analysis revealed that significantly differentially expressed genes were involved in arginine and proline metabolism and ferroptosis (Fig. 5H). Hyperoxia has been shown to reduce L-arginine levels nitric oxide generation (Yue et al., 2021). Thus, the arginine and proline metabolism pathways were verified by detecting the intracellular nitric oxide concentration. Nitric oxide concentration was significantly decreased in the HYP group, but not in the MDABP-treated group (Fig. 5B). Therefore, we hypothesized that MDABP might not exert its biological effect through the arginine and

proline metabolism pathways.

3.6. The protective effects of MDABP are associated with ferroptosis

To explore the protective function of MDABP against hyperoxia lung injury, we measured the markers of ferroptosis signaling pathway. We found that the hyperoxia group had increased cellular concentrations of Fe^{2+} and levels of oxidative indicators (ROS) and decreased activities of antioxidative indexes such as GSH compared with the normoxia group. However, the MDABP-treated group showed markedly decreased in cellular Fe^{2+} (Fig. 6A) and ROS (Fig. 6E) and increases in GSH (Fig. 6D). Furthermore, we found that 1 μM MDABP treatment significantly increased the expression of GPX4, a ferroptosis-associated protein *in vitro* (Fig. 6B and C).

3.7. MDABP ameliorates AEC injury by modulating ferroptosis

To further determine whether MDABP acts by the ferroptosis signaling pathway, we treated AEC with the ferroptosis inducer RSL3 (2 μM) (Tang et al., 2021). The results showed that MDABP had no significant effect. Conversely, RSL3 decreased cell proliferation (Fig. 7A and B) and protein expression of SP-C and AQP5 (Fig. 7F, G, I), which

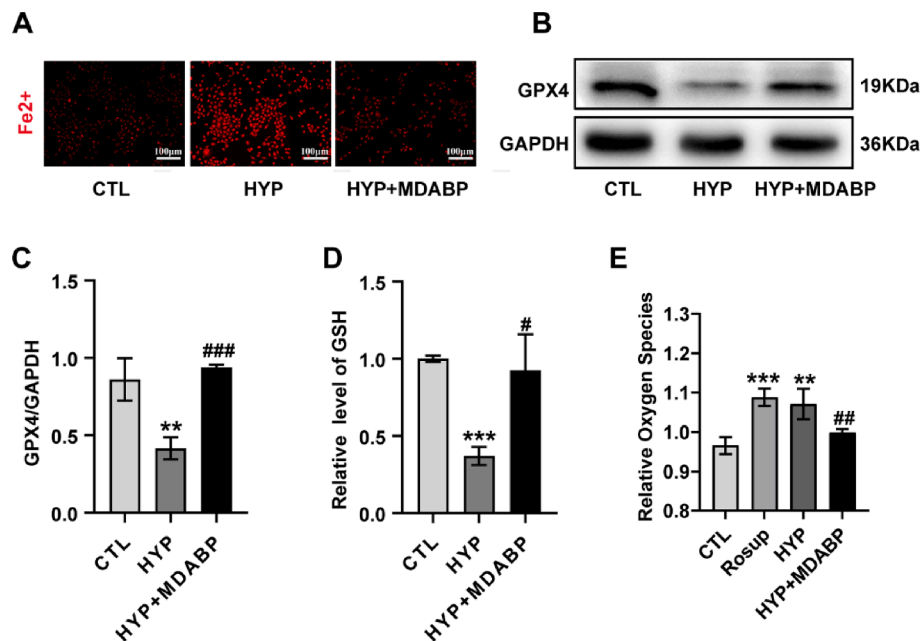


Fig. 6. The ferroptosis signaling pathway is involved in the protective effects of the peptide MDABP in vitro. (A) FerroOrange fluorescent probe was used for fluorescence imaging of Fe^{2+} in living cells. Original magnification: 100 \times . (B–C) The expression of GPX4 in A549 cells was measured by Western blotting. (D) The GSH content in A549 cells was measured by a GSH assay kit. (E) The level of ROS was examined by an ROS assay kit. Data are presented as the mean \pm SD, $n \geq 3$, */# $P < 0.05$, **/## $P < 0.01$, ***/### $P < 0.001$, ns ≥ 0.05 , * vs control group (CTL), # vs hyperoxia group (HYP).

were restored by MDABP treatment. In addition, we assessed ROS, GSH, Fe^{2+} and GPX4, a ferroptosis-associated protein, after RSL3 treatment. RSL3 increased Fe^{2+} (Fig. 7C) and ROS levels (Fig. 7E), and decreased GSH (Fig. 7D) and GPX4 expression (Fig. 7H and I), compared with the control group, but MDABP treatment reversed these effects. These results suggested that MDABP enhanced cell proliferation by inhibiting ferroptosis, thereby improving AEC injury induced by RSL3.

4. Discussion

Despite the significant advances in perinatal care over the past several decades, there is still a high incidence of BPD without an effective prevention or treatment. BPD results from impaired lung vascular and alveolar development leading to defective gas exchange (Baker et al., 2012). Thus, protecting AEC and pulmonary endothelial cells is a strategy for BPD therapy. Continuous hyperoxia exposure has been shown to cause AEC damage and reduce vascular density (Giusto et al., 2021). Thus, in this study, we used newborn SD rats to construct models of BPD through long-term exposure to high levels of oxygen.

Many bioactive peptides with diagnostic or therapeutic applications for neonatal diseases have been identified. Apelin, which has vasodilator and angiogenic effects, attenuates pulmonary inflammation, fibrin deposition, and right ventricular hypertrophy, and improves alveolarization in neonatal hyperoxic lung injury rats through a nitric oxide synthase-dependent mechanism (Bell et al., 2022). CGRP also alleviated hyperoxia-induced lung injury by enhancing cell viability and inhibiting the transdifferentiation of AECIIs. This is significantly associated with lower MDA levels, higher SOD activity, and Notch pathway activation (Deng et al., 2022).

In recent years, milk-derived bioactive peptides also have immunoregulatory, antioxidant, antimicrobial and probiotic effects that have drawn much attention (Wada and Lönnerdal, 2020). For example, BCCY-1, a β -casein-derived peptide, modulates innate immunity by activating the NF- κ B and MAPK signaling pathways (Cai et al., 2021). In addition, YVEEL, a HIV-1 TAT (48–60)-hybrid peptide, protected against experimental NEC in vitro and in vivo, by suppressing TLR4-mediated signaling through a PI3K/AKT-dependent pathway (Yan

et al., 2022). These studies demonstrate that human breast milk-derived peptides could be a potential drug for BPD therapy. We have confirmed that MDABP is the up-regulated expression in the colostrum of preterm infants, but its role in BPD remains unknown. Thus, in this study, we verified the biological characteristics and explored the effects of MDABP on BPD in vivo and in vitro. The results revealed that MDABP treatment promoted body weights of infant rats increasing, improved alveolar simplification and pulmonary vascular retardation, promoted AEC proliferation, inhibited cell apoptosis, and reduced inflammation. These data indicate that MDABP inhibits the progression of BPD.

RNA sequencing was performed to further explore the specific mechanism of MDAB on BPD. The result showed that the ferroptosis signaling pathway played a major role. The pathogenesis of BPD is very complex and it involves various factors and signaling pathways. The Notch (Tsao et al., 2016); Wnt/ β -catenin (Yang et al., 2021), Nrf2 (Amata et al., 2017) and ferroptosis signaling pathways (Chou and Chen, 2022) are involved in hyperoxia-induced lung injury. Ferroptosis, an iron-dependent form of non-apoptotic cell death, has attracted increasing interest recently. Excess iron and lipid peroxidation have been associated with BPD development (Patel et al., 2019; Ogihara et al., 1999; Baraldi et al., 2016). ROS, lipid peroxidation and accumulation of free iron are key factors in ferroptosis pathway. In this study, we found that MDABP reduced the levels of Fe^{2+} and ROS and increased GSH and GPX4 in vitro, while the ferroptosis agonist RSL3 reversed these effects. These results indicate a important role for ferroptosis in BPD and are congruent with previous studies (Jia et al., 2021).

Ferroptosis has been implicated in lung injury (Li et al., 2020; Zhang et al., 2022). However, ferroptosis and hyperoxia-induced BPD have been rarely reported (Chou and Chen, 2022). This study revealed the relationship a link between milk-derived peptides and BPD which is that promotes cell proliferation to alleviate hyperoxia-induced lung injury by inhibiting ferroptosis pathway signaling. However, this study also has some limitations. The relationship between ferroptosis and BPD has only been studied in cells and animals, and no clinical study on BPD has been conducted yet. Moreover, we used a single cell line and did not elucidate the specific mechanism of ferroptosis in hyperoxia-induced lung injury. Nrf2 is known to plays a key role in antioxidant responses and regulate

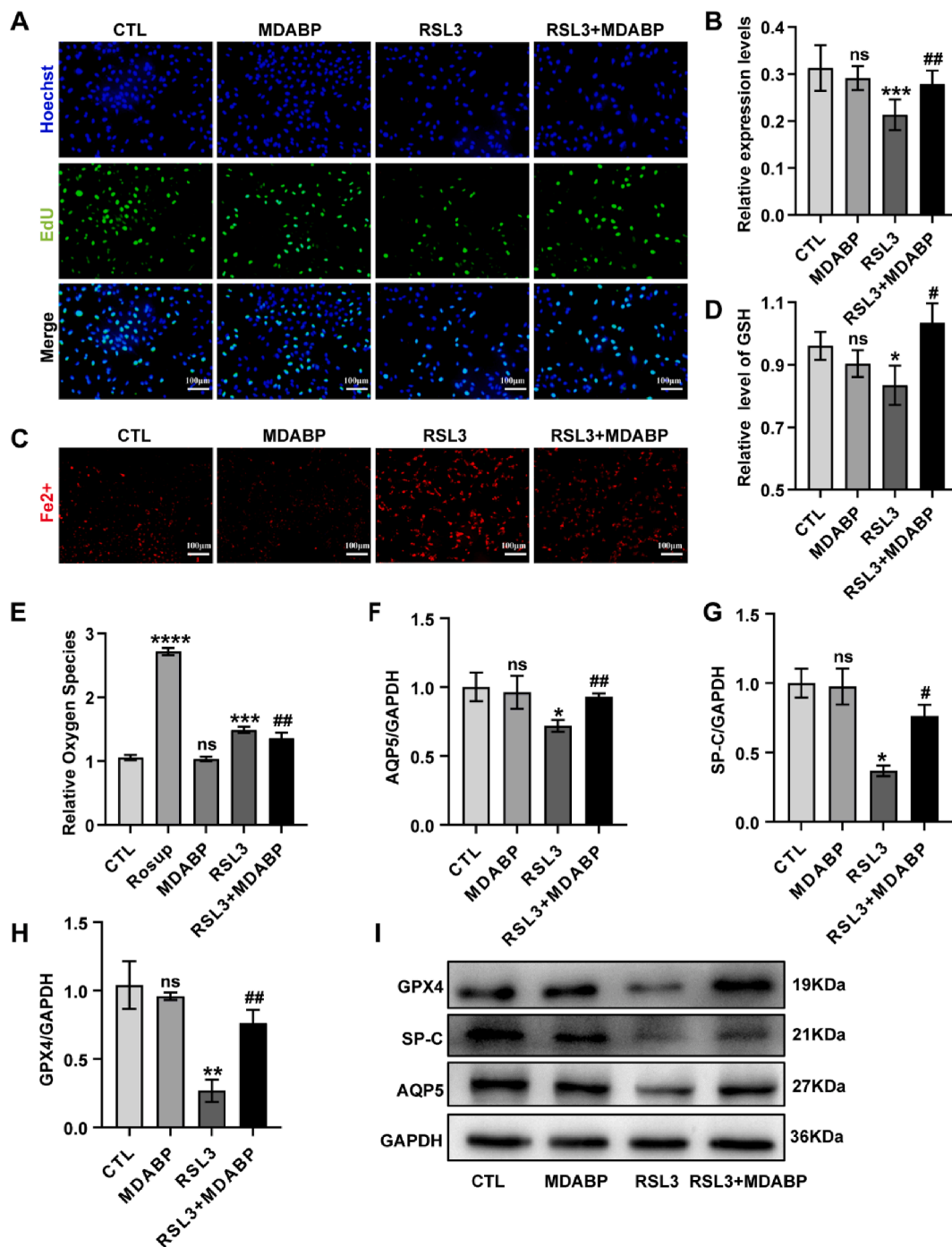


Fig. 7. MDABP rescued the alveolar epithelial cell damage caused by activation of the ferroptosis signaling pathway. RSL3 (2 μ mol/L) was used to activate the ferroptosis signaling pathway. (A-B) The cell proliferation was measured by a BeyoClick TM EdU-488 kit and the image magnification was 200 \times for each of four groups. (C) FerroOrange fluorescent probe was used for fluorescence imaging of Fe²⁺ in living cells. Original magnification: 100 \times . (D) The GSH content in A549 cells was measured by a GSH assay kit. (E) The levels of ROS were examined by an ROS assay kit. (F-I) The expression levels of AQP5, SP-C and GPX4 in A549 cells were measured by Western blotting. Data are presented as the mean \pm SD, $n \geq 6$, */ $\#$ $P < 0.05$, **/ $\#$ $P < 0.01$, ***/ $\#$ $P < 0.001$, ****/ $\#$ $P < 0.0001$, ns ≥ 0.05 , * vs control group (CTL), # vs RSL3 group.

the glutamate-cysteine reverse transport system involving xCT and GPX4, two critical targets for inhibiting ferroptosis (Dodson et al., 2019). The Nrf2/HO-1 axis also protects postnatal alveolar development (Amata et al., 2017). Panaxydol has been shown to inhibit ferroptosis by activating the KEAP1/Nrf2/HO-1 pathway, thereby reducing LPS-induced acute lung injury (Li et al., 2021). Therefore, we hypothesize that MDABP could alleviate BPD by modulating the Nrf2/HO-1 axis to suppress GSH/GPX4, a key antioxidative system in ferroptosis.

In a follow up study, our research group will collect lung tissue from patients with clinical BPD to verify that ferroptosis is involved in the pathogenesis of BPD. We will also conduct a detailed investigation of the specific mechanisms by which ferroptosis contributes to lung injury and inflammation.

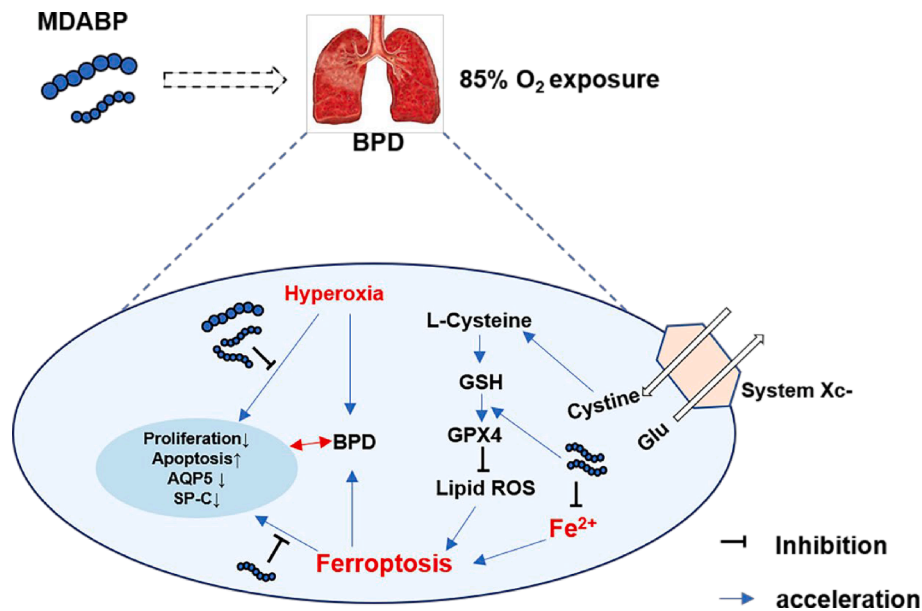


Fig. 8. Scheme illustrating the protective effects of the peptide MDABP on experimental BPD. MDABP exhibited protective effects against experimental BPD by inhibiting ferroptosis signaling pathway. Milk-Derived Anti-BPD Peptide (MDABP); Bronchopulmonary dysplasia (BPD); Aquaporin 5 (AQP5); Surfactant protein C (SP-C); Glutathione (GSH); Glutathione Peroxidase 4 (GPX4); Reactive oxygen species (ROS); Ferrous ion (Fe^{2+}).

5. Conclusions

To sum up, the human milk-derived peptide MDABP protected against experimental BPD *in vitro* and *in vivo* by inhibiting the ferroptosis signaling pathway (Fig. 8). These findings provide a unique perspective for developing innovative therapeutic agents for BPD.

Author contributions

Liu Linjie, Qian Yun and Yu Ziwei contributed equally to this work and should be considered co-first authors. Liu Linjie and Qian Yun conceived and designed the study. Liu Linjie, Yu Ziwei, Li Huimin, Chen Jingjing and Dou Heng performed the experiments. Liu Linjie, Qian Yun and Li Shushu drafted the paper. Li Shushu, Yin Jing and Han Shuping critically revised the paper. All authors read and approved the final version of the paper.

This work was supported by the Natural Science Foundation of China (82001597) and Science and Technology development Foundation of Nanjing Medical University (NMUB20220086).

CRediT authorship contribution statement

Linjie Liu: Writing – original draft, Software, Project administration, Methodology, Investigation, Data curation. **Yun Qian:** Resources, Project administration, Methodology, Investigation, Data curation. **Ziwei Yu:** Software, Methodology, Investigation. **Huimin Li:** Validation, Project administration, Methodology. **Jingjing Chen:** Validation, Software, Resources, Project administration, Methodology, Investigation. **Heng Dou:** Software, Methodology, Investigation, Data curation. **Shushu Li:** Writing – review & editing, Visualization, Validation, Supervision, Conceptualization. **Jing Yin:** Writing – review & editing, Supervision, Resources, Conceptualization. **Shuping Han:** Writing – review & editing, Validation, Supervision, Resources, Project administration, Conceptualization.

Declaration of competing interest

The authors declare that they have no known competing financial interests or personal relationships that could have appeared to influence

the work reported in this paper.

Data availability

Data will be made available on request.

References

- Amata, E., Pittalà, V., Marrazzo, A., Parenti, C., Prezzavento, O., Arena, E., Nabavi, S. M., & Salerno, L. (2017). Role of the Nrf2/HO-1 axis in bronchopulmonary dysplasia and hyperoxic lung injuries. *Clinical Science (London, England)*, 131(14), 1701–1712. <https://doi.org/10.1042/CS20170157>
- Baker, C. D., Balasubramaniam, V., Mourani, P. M., Sontag, M. K., Black, C. P., Ryan, S. L., & Abman, S. H. (2012). Cord blood angiogenic progenitor cells are decreased in bronchopulmonary dysplasia. *The European Respiratory Journal*, 40(6), 1516–1522. <https://doi.org/10.1183/09031936.00017312>
- Baraldi, E., Giordano, G., Stocchero, M., Moschino, L., Zaramella, P., Tran, M. R., Carraro, S., Romero, R., & Gervasi, M. T. (2016). Untargeted Metabolomic Analysis of Amniotic Fluid in the Prediction of Preterm Delivery and Bronchopulmonary Dysplasia. *PLoS One*, 11(10), e0164211.
- Bell EF, Hintz SR, Hansen NI, Bann CM, Wyckoff MH, DeMauro SB, Walsh MC, Vohr BR, Stoll BJ, Carlo WA, Van Meurs KP, Rysavy MA, Patel RM, Merhar SL, Sánchez PJ, Laptook AR, Hibbs AM, Cotten CM, D'Angio CT, Winter S, Fuller J, Das A; Eunice Kennedy Shriver National Institute of Child Health and Human Development Neonatal Research Network. Mortality, In-Hospital Morbidity, Care Practices, and 2-Year Outcomes for Extremely Preterm Infants in the US, 2013–2018. *JAMA*. 2022 Jan 18;327(3):248–263. doi: 10.1001/jama.2021.23580.
- Cai, J., Li, X., Wang, X., Jiang, C., Shen, D., Cui, X., Xie, K., Ji, C., & Cao, Y. (2021). A human β -casein-derived peptide BCCY-1 modulates the innate immune response. *Food Chemistry*, 30(348), Article 129111. <https://doi.org/10.1016/j.foodchem.2021.129111>
- Chou, H. C., & Chen, C. M. (2022). Hyperoxia Induces Ferroptosis and Impairs Lung Development in Neonatal Mice. *Antioxidants (Basel)*, 11(4), 641. <https://doi.org/10.3390/antiox11040641>
- Chou, H. C., & Chen, C. M. (2022). Cathelicidin Attenuates Hyperoxia-Induced Lung Injury by Inhibiting Ferroptosis in Newborn Rats. *Antioxidants (Basel)*, 11(12), 2405. <https://doi.org/10.3390/antiox11122405>
- Dakshinamurti, S. (2022). Thrombospondin in the Puzzle of Bronchopulmonary Dysplasia. *American Journal of Respiratory and Critical Care Medicine*, 205(6), 610–612. <https://doi.org/10.1164/rccm>
- Dang, H. X., Li, J., Liu, C., Fu, Y., Zhou, F., Tang, L., Li, L., & Xu, F. (2017). CGRP attenuates hyperoxia-induced oxidative stress-related injury to alveolar epithelial type II cells via the activation of the Sonic hedgehog pathway. *International Journal of Molecular Medicine*, 40(1), 209–216. <https://doi.org/10.3892/ijmm.2017.3002>
- Deng, X., Bao, Z., Yang, X., Mei, Y., Zhou, Q., Chen, A., Yu, R., & Zhang, Y. (2023). Molecular mechanisms of cell death in bronchopulmonary dysplasia. *Apoptosis*, 28(1–2), 39–54. <https://doi.org/10.1007/s10495-022-01791-4>
- Deng, J., Wang, S. H., Zheng, X. M., & Tang, Z. M. (2022). Calcitonin Gene-Related Peptide Attenuates Hyperoxia-Induced Oxidative Damage in Alveolar Epithelial

- Type II Cells Through Regulating Viability and Transdifferentiation. *Inflammation*, 45 (2), 863–875. <https://doi.org/10.1007/s10753-021-01591-z>
- Dodson, M., Castro-Portuguez, R., & Zhang, D. D. (2019). NRF2 plays a critical role in mitigating lipid peroxidation and ferroptosis. *Redox Biology*, 23, Article 101107. <https://doi.org/10.1016/j.redox.2019.101107>
- Fu, Y., Ji, C., Chen, X., Cui, X., Wang, X., Feng, J., Li, Y., Qin, R., & Guo, X. (2017). Investigation into the antimicrobial action and mechanism of a novel endogenous peptide β -casein 197 from human milk. *AMB Express*, 7(1), 119. <https://doi.org/10.1186/s13568-017-0409-y>
- Gilfillan, M., Bhandari, A., & Bhandari, V. (2021). Diagnosis and management of bronchopulmonary dysplasia. *BMJ*, 20(375), Article n1974. <https://doi.org/10.1136/bmj.n1974>
- Giusto K, Wanczyk H, Jensen T, Finck C. Hyperoxia-induced bronchopulmonary dysplasia: better models for better therapies. *Dis Model Mech*. 2021 Feb 23;14(2): dmm047753. doi: 10.1242/dmm.047753.
- Hamley, I. W. (2017). Small bioactive peptides for biomaterials design and therapeutics. *Chemical Reviews*, 117(24), 14015–14041. <https://doi.org/10.1021/acs.chemrev.7b00522>
- Huang, J., Zhang, L., Tang, J., Shi, J., Qu, Y., Xiong, T., & Mu, D. (2019). Human milk as a protective factor for bronchopulmonary dysplasia: A systematic review and meta-analysis. *Archives of Disease in Childhood-Fetal and Neonatal Edition*, 104(2), F128–F136. <https://doi.org/10.1136/archdischild-2017-314205>
- Jia, D., Zheng, J., Zhou, Y., Jia, J., Ye, X., Zhou, B., Chen, X., Mo, Y., & Wang, J. (2021). Ferroptosis is Involved in Hyperoxic Lung Injury in Neonatal Rats. *Journal of Inflammation Research*, 18(14), 5393–5401. <https://doi.org/10.2147/JIR.S335061>
- Li, Y., Cao, Y., Xiao, J., Shang, J., Tan, Q., Ping, F., Huang, W., Wu, F., Zhang, H., & Zhang, X. (2020). Inhibitor of apoptosis-stimulating protein of p53 inhibits ferroptosis and alleviates intestinal ischemia/reperfusion-induced acute lung injury. *Cell Death and Differentiation*, 27(9), 2635–2650. <https://doi.org/10.1038/s41418-020-0528-x>
- Li, J., Lu, K., Sun, F., Tan, S., Zhang, X., Sheng, W., Hao, W., Liu, M., Lv, W., & Han, W. (2021). Panaxydol attenuates ferroptosis against LPS-induced acute lung injury in mice by Keap1-Nrf2/HO-1 pathway. *Journal of Translational Medicine*, 19(1), 96. <https://doi.org/10.1186/s12967-021-02745-1>
- Liu, Y., Lu, J., Wang, X., Chen, L., Liu, S., Zhang, Z., & Yao, W. (2017). Erythropoietin-derived peptide protects against acute lung injury after rat traumatic brain injury. *Cellular Physiology and Biochemistry*, 41(5), 2037–2044. <https://doi.org/10.1159/000475434>
- Ogihara, T., Hirano, K., Morinobu, T., Kim, H. S., Hiroi, M., Ogihara, H., & Tamai, H. (1999). Raised concentrations of aldehyde lipid peroxidation products in premature infants with chronic lung disease. *Archives of Disease in Childhood-Fetal and Neonatal Edition*, 80(1), F21–F25. <https://doi.org/10.1136/fn.80.1.f21>
- Patel, R. M., Knezevic, A., Yang, J., Shenvi, N., Hinkes, M., Roback, J. D., Easley, K. A., & Josephson, C. D. (2019). Enteral iron supplementation, red blood cell transfusion, and risk of bronchopulmonary dysplasia in very-low-birth-weight infants. *Transfusion*, 59(5), 1675–1682. <https://doi.org/10.1111/trf.15216>
- Tang, Z., Jiang, W., Mao, M., Zhao, J., Chen, J., & Cheng, N. (2021). Deubiquitinase USP35 modulates ferroptosis in lung cancer via targeting ferroportin. *Clinical and Translational Medicine*, 11(4), e390.
- Thébaud, B., Goss, K. N., Laughon, M., Whitsett, J. A., Abman, S. H., Steinhorn, R. H., Aschner, J. L., Davis, P. G., McGrath-Morrow, S. A., Soll, R. F., & Jobe, A. H. (2019). Bronchopulmonary dysplasia. *Nature Reviews Disease Primers*, 5(1), 78. <https://doi.org/10.1038/s41572-019-0127-7>
- Tsao, P. N., Matsuoka, C., Wei, S. C., Sato, A., Sato, S., Hasegawa, K., Chen, H. K., Ling, T. Y., Mori, M., Cardoso, W. V., & Morimoto, M. (2016). Epithelial Notch signaling regulates lung alveolar morphogenesis and airway epithelial integrity. *Proceedings of the National Academy of Sciences of the United States of America*, 113 (29), 8242–8247. <https://doi.org/10.1073/pnas.1511236113>
- Villamor-Martínez, E., Pierro, M., Cavallaro, G., Mosca, F., Kramer, B. W., & Villamor, E. (2018). Donor Human Milk Protects against Bronchopulmonary Dysplasia: A Systematic Review and Meta-Analysis. *Nutrients*, 10(2), 238. <https://doi.org/10.3390/nu10020238>
- Visser, Y. P., Walther, F. J., Laghmani el, H., Av, L., & Wagenaar, G. T. (2010). Apelin attenuates hyperoxic lung and heart injury in neonatal rats. *American Journal of Respiratory and Critical Care Medicine*, 182(10), 1239–1250. <https://doi.org/10.1164/rccm.200909-1361OC>
- Wada, Y., & Lönnérda, B. (2020). Bioactive peptides derived from human milk proteins: An update. *Current Opinion in Clinical Nutrition and Metabolic Care*, 23(3), 217–222. <https://doi.org/10.1097/MCO.0000000000000642>
- Wang, X., Yan, X., Zhang, L., Cai, J., Zhou, Y., Liu, H., Hu, Y., Chen, W., Xu, S., Liu, P., Chen, T., Zhang, J., Cao, Y., Yu, Z., & Han, S. (2019). Identification and peptidomic profiling of exosomes in preterm human Milk: Insights into necrotizing enterocolitis prevention. *Molecular Nutrition & Food Research*, 63(13), e1801247.
- Yan, X., Cao, Y., Chen, W., Yu, Q., Chen, Y., Yao, S., Jiang, C., Chen, X., & Han, S. (2022). Peptide Tat(48–60) YVEEL protects against necrotizing enterocolitis through inhibition of toll-like receptor 4-mediated signaling in a phosphatidylinositol 3-kinase/AKT dependent manner. *Frontiers in Nutrition*, 10(9), Article 992145. <https://doi.org/10.3389/fnut.2022.992145>
- Yang, M., Gao, X. R., Meng, Y. N., Shen, F., & Chen, Y. P. (2021). ETS1 Ameliorates Hyperoxia-Induced Alveolar Epithelial Cell Injury by Regulating the TGM2-Mediated Wnt/ β -Catenin Pathway. *Lung*, 199(6), 681–690. <https://doi.org/10.1007/s00408-021-00489-9>
- Yi, D. Y., & Kim, S. Y. (2021). Human breast milk composition and function in human health: from nutritional components to microbiome and MicroRNAs. *Nutrients*, 13 (9), 3094. <https://doi.org/10.3390/nu13093094>
- Yue, L., Lu, X., Dennery, P. A., & Yao, H. (2021). Metabolic dysregulation in bronchopulmonary dysplasia: Implications for identification of biomarkers and therapeutic approaches. *Redox Biology*, 48, Article 102104. <https://doi.org/10.1016/j.redox.2021.102104>
- Zhang, H., Liu, J., Zhou, Y., Qu, M., Wang, Y., Guo, K., Shen, R., Sun, Z., Cata, J. P., Yang, S., Chen, W., & Miao, C. (2022). Neutrophil extracellular traps mediate m⁶A modification and regulates sepsis-associated acute lung injury by activating ferroptosis in alveolar epithelial cells. *International Journal of Biological Sciences*, 18 (8), 3337–3357. <https://doi.org/10.7150/ijbs.69141>
- Zhou, Y., Liu, Y., Xu, G., Liu, L., Li, H., Li, Y., Yin, J., Wang, X., & Yu, Z. (2022). Human breast milk-derived exosomes through inhibiting AT II cell apoptosis to prevent bronchopulmonary dysplasia in rat lung. *Journal of Cellular and Molecular Medicine*, 26(15), 4169–4182. <https://doi.org/10.1111/jcmm.17334>